

## REIONIZATION HISTORIES OF MILKY WAY MASS HALOS

TONY Y. LI<sup>1</sup>, MARCELO A. ALVAREZ<sup>2</sup>, RISA H. WECHSLER<sup>1</sup>, TOM ABEL<sup>1</sup>

<sup>1</sup>Kavli Institute for Particle Astrophysics and Cosmology; Physics Department, Stanford University, Stanford, CA 94305, USA  
SLAC National Accelerator Laboratory, Menlo Park, CA 94025, USA;  
tonyyli@stanford.edu, rwechsler@stanford.edu, tabel@stanford.edu

<sup>2</sup>CITA, University of Toronto, Toronto, Ontario, Canada; malvarez@cita.utoronto.ca

(Dated: November 24, 2018)  
Draft version November 24, 2018

### ABSTRACT

We investigate the connection between the epoch of reionization and the present day universe, by examining the extended mass reionization histories of dark matter halos identified at  $z = 0$ . We combine an N-body dark matter simulation of a 600 Mpc volume with a three-dimensional, seminumerical reionization model. This provides reionization redshifts for each particle, which can then be connected with the properties of their halos at the present time. We find that the vast majority of present-day halos with masses larger than  $\sim \text{few} \times 10^{11} M_{\odot}$  reionize earlier than the rest of the universe. We also find significant halo-to-halo diversity in mass reionization histories, and find that in realistic inhomogeneous models, the material within a given halo is not expected to reionize at the same time. In particular, the scatter in reionization times *within* individual halos is typically larger than the scatter *among* halos. From our fiducial reionization model, we find that the typical 68% scatter in reionization times within halos is  $\sim 115$  Myr for  $10^{12 \pm 0.25} M_{\odot}$  halos, decreasing slightly to  $\sim 95$  Myr for  $10^{15 \pm 0.25} M_{\odot}$  halos. We find a mild correlation between reionization history and environment: halos with shorter reionization histories are typically in more clustered environments, with the strongest trend on a scale of  $\sim 20$  Mpc. Material in Milky Way mass halos with short reionization histories is preferentially reionized in relatively large HII regions, implying reionization mostly by sources external to the progenitors of the present-day halo. We investigate the impact on our results of varying the reionization model parameters, which span a range of reionization scenarios with varying timing and morphology.

*Subject headings:* reionization — cosmology: theory — galaxies: formation — dark matter

### 1. INTRODUCTION

The signs of reionization should survive to the present day universe. Although the epoch of reionization is constrained to redshifts  $z \gtrsim 6$  by quasar absorption spectra (e.g., Becker et al. 2001; Fan et al. 2006) and the cosmic microwave background (Komatsu et al. 2011; Hinshaw et al. 2012), the process is likely to be temporally extended and spatially inhomogeneous (Gnedin 2000a; Miralda-Escudé et al. 2000; Sokasian et al. 2001; Barkana & Loeb 2004; Iliev et al. 2006; Trac & Cen 2007). One also expects the process to be closely coupled to the formation of early galaxies: on one hand, high-redshift, low-mass galaxies may be essential sources of ionizing radiation (e.g., Wise & Cen 2009; Bouwens et al. 2012; Kuhlen & Faucher-Giguère 2012; Alvarez et al. 2012). On the other hand, reionization may photoheat gas in halos with virial temperatures  $T_{\text{vir}} \lesssim 10^4$  K, suppressing or truncating galaxy formation in those low-mass halos (Efstathiou 1992; Shapiro et al. 1994; Thoul & Weinberg 1996; Barkana & Loeb 1999; Gnedin 2000b; Dijkstra et al. 2004; Okamoto et al. 2008).

Indeed, this proposed suppression of galaxy formation may partially alleviate the so-called “missing satellites” problem (Moore et al. 1999; Klypin et al. 1999; Bullock et al. 2000; Kravtsov et al. 2004), in which cold dark matter simulations predict far more dark matter subhalos in the Local Group than observed satellite galaxies. Reionization provides a plausible mechanism for suppressing the present-day faint satellite population, reducing the missing satellite discrepancy. Recently, the discovery of so-called “ultra-faint dwarf” galaxies around

the Milky Way (e.g., Willman et al. 2005; Zucker et al. 2006; Belokurov et al. 2007) has partially closed the gap. However, there is also evidence that their star formation histories may have been truncated during reionization (Brown et al. 2012). If, indeed, reionization directly affects the present-day population of faint satellites (Koposov et al. 2009; Busha et al. 2010; Ocvirk & Aubert 2011), or leaves its mark in other ways, then it is important to quantify the reionization epoch and history of the Local Group environment (Weinmann et al. 2007; Iliev et al. 2011).

Self-consistently modeling the competing, simultaneous processes involved in reionization will be a key component of a comprehensive theory of galaxy formation. In particular, three-dimensional simulations are necessary to capture the patchy morphology and evolution of the ionized HII regions. Unfortunately, the ideal of direct, radiative transfer simulations of reionization, over all scales involved, is prohibitively expensive on present-day computers. However, insofar as we would like to model the large scale morphology of reionized regions, approximate seminumerical schemes have shown good agreement with radiative transfer simulations, on large scales, at a fraction of the computational cost (Zahn et al. 2007, 2011; Santos et al. 2010; Mesinger et al. 2011).

A number of previous studies have directly informed our focus here. Alvarez et al. (2009) combined three-dimensional reionization calculations with an N-body simulation to assign reionization epochs to present-day dark matter halos. Busha et al. (2010) applied the resulting distribution of reionization

redshifts to Via Lactea II subhalo catalogs, finding that varying the Milky Way reionization epoch could alter the satellite population of Milky Way halos by up to 2 orders of magnitude, while assuming for simplicity that the halo reionization epoch was instantaneous. Lunnan et al. (2012), using a similar method for calculating satellite luminosities, explicitly modeled the effect of patchy reionization on the satellite population of six Milky Way-like halos. Comparing instantaneous and inhomogeneous reionization scenarios, they found differences of 10-20%—both increase and decrease—in the number of faint ( $M_V \gtrsim -10$ ) satellites, suggesting against a systematic correction between the two scenarios. Additionally, they found a large halo-to-halo scatter in satellite populations across a small sample of 6 halos, motivating the study of a larger, statistical sample of halos.

In order to further investigate and quantify the connection between patchy reionization and present-day halos, we have therefore chosen an N-body simulation which includes both (1) well-resolved  $z = 0$  halos down to Milky Way masses, and (2) a large, statistical sample of such halos. In this study, we focus on calculating the *extended* reionization histories of present-day halos in order to quantify the inhomogeneity of their reionization epochs.

## 2. MODELING

### 2.1. Reionization Model

We employ a seminumerical reionization model, which we summarize here, based on the analytic prescription developed by Furlanetto et al. (2004) and extended to three dimensions by Zahn et al. (2007). We include an additional treatment of photon absorption by Lyman-limit systems, following the implementation of Alvarez & Abel (2012); further details may be found in that paper.

The fundamental assumption of the model is that a given region is completely ionized if enough photons have been emitted by enclosed sources to ionize it. Formally, in order to ionize the region we require that  $f_{\text{coll}}$ , the fraction of matter collapsed in halos above some mass threshold  $M_{\text{min}}$ , satisfies the inequality

$$\zeta f_{\text{coll}} \geq 1 \quad (1)$$

where  $f_{\text{coll}}$  is the fraction of mass in collapsed objects within the region. The efficiency factor  $\zeta$ , which may be interpreted as the effective number of ionizing photons released per collapsed atom, encapsulates all galaxy formation and radiative transfer physics. Via the excursion-set formalism (e.g., Bond et al. 1991; Lacey & Cole 1993),  $f_{\text{coll}}$  in a spherical region of mass  $m$  and overdensity  $\delta$  may be written

$$f_{\text{coll}} = \text{erfc} \left\{ \frac{\delta_c(z) - \delta_m}{\sqrt{2[\sigma^2(M_{\text{min}}) - \sigma^2(m)]}} \right\}. \quad (2)$$

At any given position, the density field is smoothed with a spherical real-space top hat filter, over increasing radii  $R$  (or alternatively mass scales  $m$ ), and the earliest redshift, at any smoothing scale, for which Equation 1 is satisfied is recorded as the reionization redshift  $z_{\text{reion}}$  of that point. To ensure global photon conservation, we follow the procedure also outlined in Alvarez & Abel (2012), in which the reionization redshift of each cell is modified so that the order in which cells

TABLE 1  
REIONIZATION MODEL PARAMETERS

$\tau_{\text{es}}$ <sup>a</sup>	$M_{\text{min}} [M_{\odot}]$ <sup>b</sup>	$\lambda_{\text{abs}} [\text{Mpc } h^{-1}]$ <sup>c</sup>	$\zeta$ <sup>d</sup>	$z_{0.5}$ <sup>e</sup>	$z_{\text{end}}$ <sup>f</sup>
0.06	$10^8$	8	18.1	8.4	3.6
0.06	$10^8$	32	14.6	8.3	4.9
0.06	$10^8$	256	13.1	8.2	6.4
0.06	$10^9$	8	72.9	8.5	5.3
0.06	$10^9$	32	56.0	8.4	6.0
0.06	$10^9$	256	50.0	8.3	7.1
0.09	$10^8$	8	113.0	11.3	7.7
<b>g 0.09</b>	<b><math>10^8</math></b>	<b>32</b>	<b>90.9</b>	<b>11.2</b>	<b>8.5</b>
0.09	$10^8$	256	81.0	11.1	9.7
0.09	$10^9$	8	1020.0	11.4	9.0
0.09	$10^9$	32	785.0	11.3	9.5
0.09	$10^9$	256	700.0	11.3	10.3
0.12	$10^8$	8	812.0	13.9	10.9
0.12	$10^8$	32	657.0	13.8	11.6
0.12	$10^8$	256	580.0	13.8	12.5
0.12	$10^9$	8	1.82e4	14.0	12.0
0.12	$10^9$	32	1.41e4	13.9	12.4
0.12	$10^9$	256	1.24e4	13.9	13.0

<sup>a</sup>Electron scattering optical depth to reionization.

<sup>b</sup>Minimum halo mass of ionizing sources.

<sup>c</sup>Mean free path of residual Lyman absorption systems.

<sup>d</sup>Ionizing efficiency, implicitly set by other parameters.

<sup>e</sup>Redshift when global reionized mass fraction is 0.5.

<sup>f</sup>Redshift when global reionized mass fraction is 1.0.

<sup>g</sup>Bold: fiducial model.

are ionized is preserved, but the overall reionization history is given by

$$\frac{dx}{dt} = \zeta \frac{d\bar{f}_{\text{coll}}}{dt} \frac{\lambda_{\text{abs}}}{\lambda_{\text{abs}} + \lambda_{\text{b}}(x)} \quad (3)$$

where  $\bar{f}_{\text{coll}}$  is the mean collapsed fraction and  $\lambda_{\text{b}}(x)$  is the evolving mean distance between neutral patches—the "bubble mean free path" (Alvarez & Abel 2012).

To perform the calculation, the simulation box is uniformly subdivided into  $1400^3$  cells, and the smoothing procedure is performed around the center of each cell, assigning it a reionization redshift. There are exactly as many cells as simulation particles (see §2.2), linking every cell to a unique initial, unperturbed simulation particle. Because the excursion set formalism is fundamentally Lagrangian—i.e., it follows mass rather than volume elements—this directly tags each particle with its own reionization redshift  $z_{\text{reion}}$ , or alternately a look-back reionization time,  $t_{\text{reion}}$ . Assuming that baryons trace the dark matter in our simulation, this allows us to characterize the reionization times of baryonic matter in present-day halos.

Our model is parameterized by three global values:

1.  $\tau_{\text{es}}$ , the optical depth of CMB photons to scattering from free electrons
2.  $\lambda_{\text{abs}}$ , the comoving, spatially uniform mean free path of absorption systems
3.  $M_{\text{min}}$ , the minimum halo mass of ionizing sources

The ionizing efficiency  $\zeta$  is then implicitly determined from these parameters. Table 1 lists all parameter values explored,

and we briefly discuss the effect of varying these parameters in §3.4. For our fiducial model, we use  $\tau_{\text{es}} = 0.09$ ,  $\lambda_{\text{abs}} = 32 \text{ Mpc } h^{-1}$ ,  $M_{\text{min}} = 10^8 M_{\odot}$ , in which reionization is completed by  $z_{\text{end}} \approx 8.5$ . This is somewhat early relative to the  $z_{\text{end}} \gtrsim 6$  constraint inferred from quasar spectra, but ensures a global reionization history consistent with the inferred value of  $\tau_{\text{es}}$  from the WMAP 7-year result,  $\tau_{\text{es}} = 0.088 \pm 0.014$  (Komatsu et al. 2011) [note that it remains consistent with subsequent WMAP 9-year ( $0.081 \pm 0.012$ ) and Planck ( $0.092 \pm 0.013$ ) results (Bennett et al. 2012; Planck Collaboration et al. 2013)]. We have evaluated  $\tau_{\text{es}}$  here as:

$$\tau_{\text{es}} = \frac{3H_0\Omega_b c\sigma_T}{8\pi Gm_p} \int_0^{\infty} \frac{x(z)(1+z)^2(1-Y+N_{\text{He}}(z)Y/4)}{\sqrt{\Omega_m(1+z)^3+1-\Omega_m}} dz, \quad (4)$$

where  $Y \simeq 0.24$  is the helium abundance and  $N_{\text{He}}(z)$  is the number of times helium is ionized—we use  $N_{\text{He}} = 2$  for  $z < 3$  and  $N_{\text{He}} = 1$  for  $z > 3$ .

We acknowledge the simplicity inherent in a model, such as this one, which does not explicitly include radiative transfer. However, comparisons of radiative transfer and seminumerical codes have been performed (e.g., Zahn et al. 2011), in which both schemes predict similar HII morphologies and are in excellent agreement on scales of  $\gtrsim \text{Mpc}$ . The seminumerical scheme does so at a fraction of the computational cost, justifying its use when such large-scale reionization morphology is the main concern, as it is here.

## 2.2. *N*-Body Simulation

Although our reionization model is calculated solely from the initial overdensity field, we wish to connect those calculations to present-day halos. To that end, we use one realization of the *Consuelo* *N*-body simulations from the Large Suite of Dark Matter Simulations<sup>1</sup>. The simulation contains 1400<sup>3</sup> dark matter particles, each with mass  $m_p = 2.67 \times 10^9 M_{\odot}$ , within a comoving 600 Mpc box with periodic boundary conditions. Particles were evolved forward in time with the GADGET-2 code (Springel 2005), and in this study we assume cosmological parameters consistent with those of the simulation, namely  $\Omega_M = 0.25$ ,  $\Omega_{\Lambda} = 0.75$ ,  $h = 0.7$ ,  $\sigma_8 = 0.8$ ,  $n_s = 1.0$ .

In the simulation, dark matter halos were identified using the ROCKSTAR phase-space halo finder (Behroozi et al. 2013), which resolved  $\sim 1.6 \times 10^6$  halos in the mass range  $10^{11.25} M_{\odot} \lesssim M_{\text{halo}} \lesssim 10^{15.25} M_{\odot}$ . In this study, we have not counted another  $\sim 4.5 \times 10^5$  subhalos, i.e. halos located within the virial radius of a larger halo, as additional halos, although we note that including them does not significantly impact the particular results presented here. In the language of this paper, “Milky Way mass halos” simply refers to halos the mass range  $M_{\text{halo}} = 10^{12 \pm 0.25} M_{\odot}$ . There are  $\sim 3.8 \times 10^5$  such halos at  $z = 0$  in our volume.

We expect that the volume of our simulation should be sufficient to statistically sample the largest HII region sizes, which typically grow to tens of comoving Mpc toward the end of the reionization epoch (Furlanetto & Oh 2005; Zahn et al. 2005; Mesinger & Furlanetto 2007; Zahn et al. 2007; Shin et al. 2008).

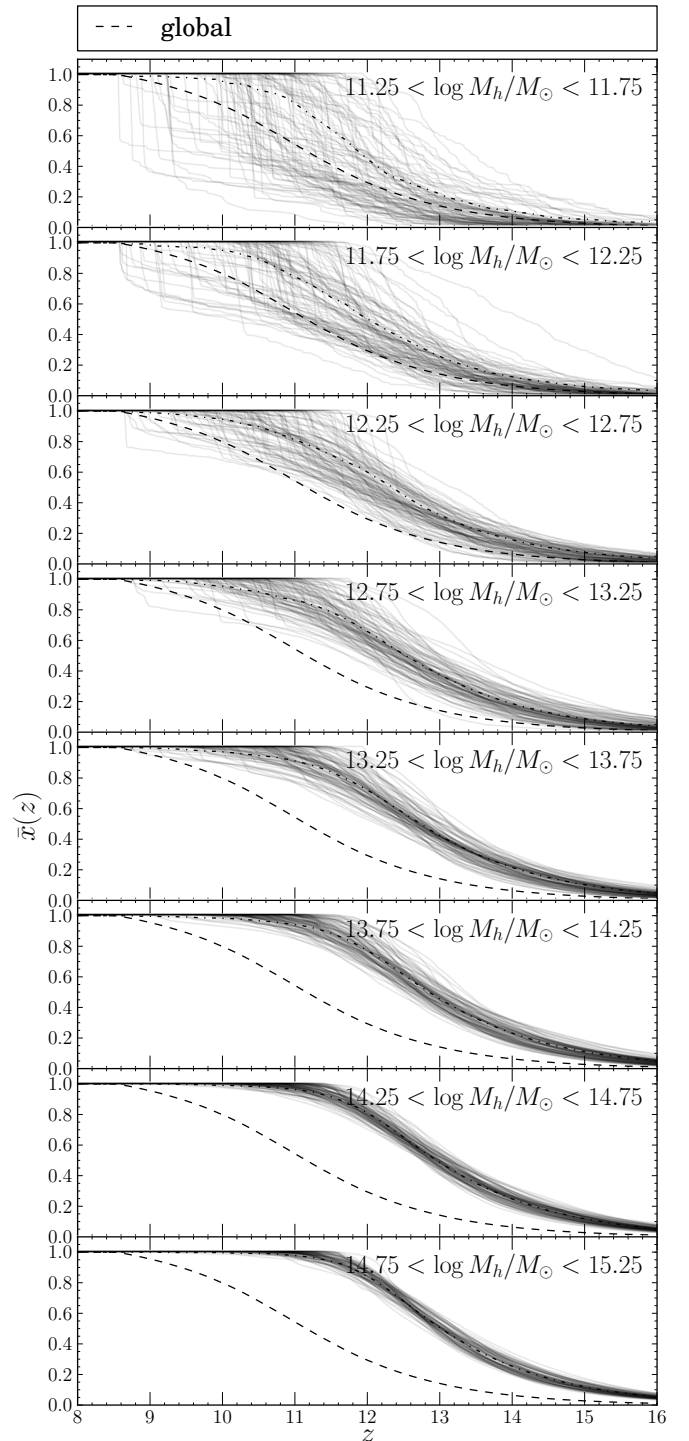


FIG. 1.— Randomly-selected halo reionization histories, in increasing mass bins of width 0.5 dex. The reionized fraction  $\bar{x}(z)$  of each halo’s  $z = 0$  mass is plotted as a function of redshift. 100 halos were selected in each mass bin. The global reionized mass fraction (*dotted*) and the mean halo reionized fraction (*dash-dotted*) are also shown in each bin.

<sup>1</sup> <http://lss.phy.vanderbilt.edu/lasdamas>

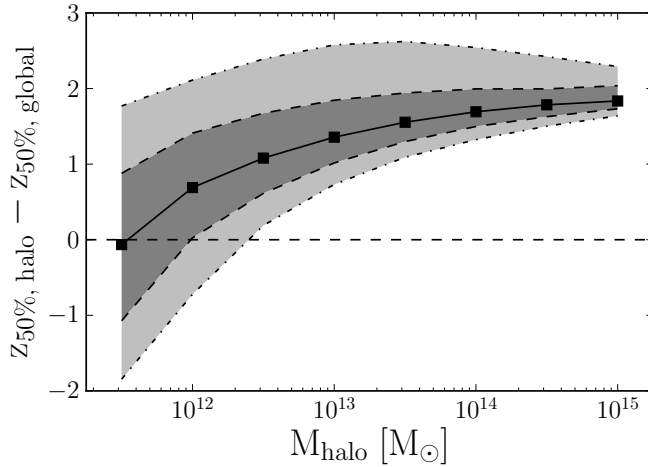


FIG. 2.— Offset between halo and global half-reionized redshifts, as a function of  $z=0$  halo mass. In each mass bin, the median (*solid black squares*) is indicated, along with lines tracing the 68% (*dashed*) and 95% (*dash-dotted*) distributions. A halo which lies above (below) the dotted line essentially reionizes before (after) the rest of the universe.

### 3. RESULTS

Having obtained a reionization time for each simulation particle, we find that the global 68% spread in reionization times across *all* particles is 150 Myr, and the spread in reionization times over all present-day *halo* particles is 130 Myr. We begin in §3.1 by quantifying the internal scatter in reionization times for halos of all masses. In §3.2 we focus on Milky Way mass halos, identifying a connection between halo reionization histories and local environment, and in §3.3, we check how additional environmental constraints, namely the presence of M31 and Virgo, affect our results. Finally, in §3.4, we briefly discuss how varying the parameters of our reionization model affects the distribution of Milky Way reionization histories.

#### 3.1. Halo Reionization Histories and Durations

Having tagged each simulation particle with a reionization redshift, we obtain reionization histories for the mass in each  $z=0$  halo. Figure 1 shows the reionized mass fraction of present-day halos as a function of redshift, for a random selection in increasing mass bins: from  $\sim 10^{11.5} M_{\odot}$  up to  $\sim 10^{15} M_{\odot}$ . For comparison, we also indicate the mean reionized fraction of halos within each mass bin as well as the global reionized mass fraction. We note that most halos have biased reionization histories, in that they reionize before the rest of the universe. The majority of  $z=0$  halos have a reionized fraction above the global fraction at any given redshift, indicating that the halos reionize early relative to the universe as a whole, or equivalently that they are spatially correlated with regions of early reionization. In Figure 2, we show this more explicitly by displaying the redshift differences between halo and global half-reionization. By this measure, most halos larger than  $\sim 10^{12} M_{\odot}$  and nearly all halos larger than  $\sim 10^{12.5} M_{\odot}$  reionized ahead of the universe. Note that the mean halo reionization fractions in Figure 1 are calculated at fixed redshifts, while Figure 2 compares halos at a fixed reionized fraction, accounting for any apparent discrepancies

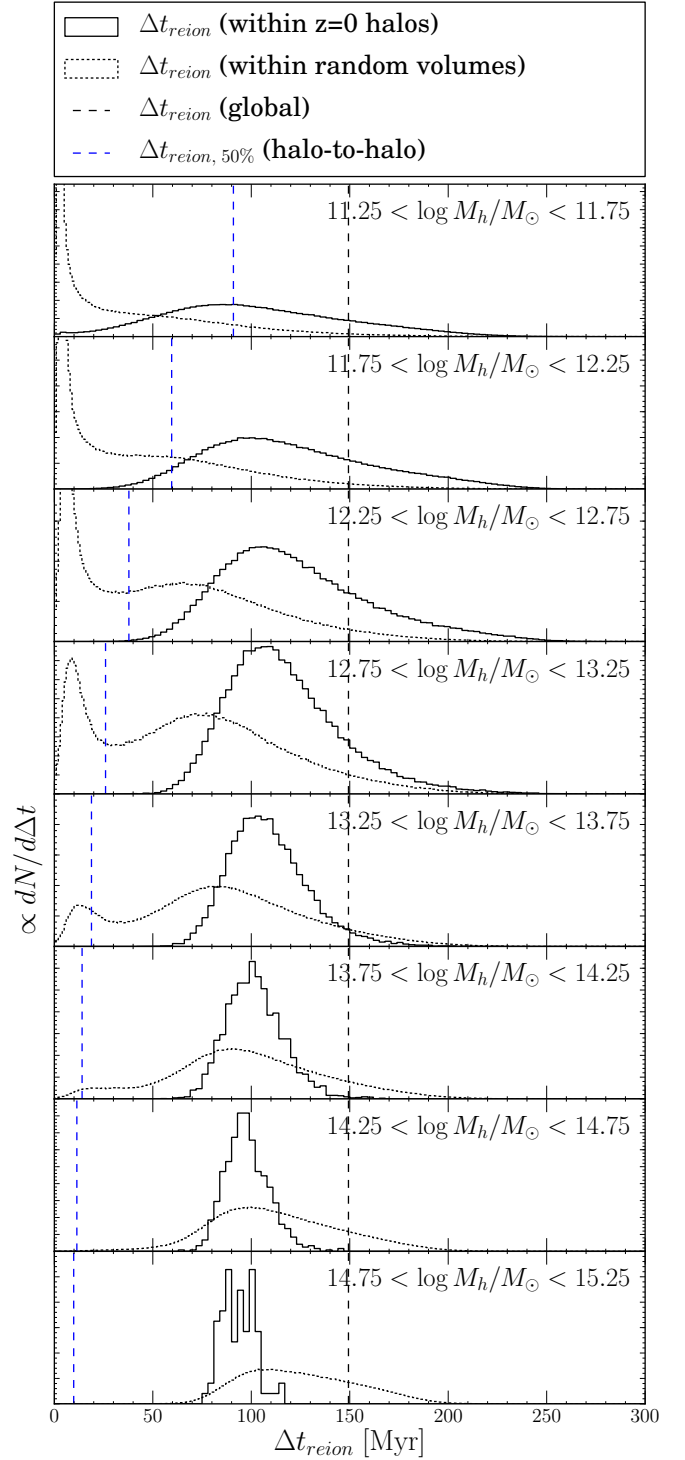


FIG. 3.— Distribution of  $\Delta t_{reion}$  within  $z=0$  halos, for our fiducial model, in increasing mass bins. Plotted for comparison are the halo-to-halo scatter in median  $z_{reion}$  (blue) and the global scatter for the all particles (black). The dotted curve represents the distribution of  $\Delta t_{reion}$  for random cubic volumes of comparable mass.

between them.

For each  $z = 0$  halo, we calculate  $\Delta t_{\text{reion}}$ , which we define as the central 68% spread in reionization times of its present-day particles, i.e. the difference between the 16th and 84th percentile of  $t_{\text{reion}}$  values within the halo. Thus, the quantity  $\Delta t_{\text{reion}}$  quantifies the  $1\sigma$  scatter in mass-weighted reionization times within a present day halo, and it may be thought of as approximately characterizing the duration of a halo’s reionization history. However, we caution against an overly simplistic picture of the process, noting that these halos were generally built up through the mergers of many smaller halos, which were themselves distinct or yet-unformed objects during the epoch of reionization.

Figure 3 shows the distribution of  $\Delta t_{\text{reion}}$  for all halos in our fiducial reionization model, also in logarithmically spaced mass bins, from  $\sim 10^{11.5} M_{\odot}$  up to  $\sim 10^{15} M_{\odot}$ . We find that the median  $\Delta t_{\text{reion}}$  is about 100 Myr for  $\sim 10^{11.5} M_{\odot}$  halos, rising to 115 Myr for  $\sim 10^{12} M_{\odot}$  halos, then decreasing weakly with halo mass to 95 Myr for  $\sim 10^{15} M_{\odot}$  halos. For comparison, the 68% scatter in median reionization times *across* halos is plotted in each mass bin, decreasing from  $\sim 90$  Myr to  $\sim 10$  Myr over the same mass range. Significantly,  $\Delta t_{\text{reion}}$ , the scatter in  $t_{\text{reion}}$  *within* halos, is typically larger than the same scatter in median  $t_{\text{reion}}$  across halos: reionization epochs within present-day halos are typically more variable within, rather than across, halos of similar mass.

For further comparison, Figure 3 also shows the distribution  $\Delta t_{\text{reion}}$  for completely *random* cubic volumes with equivalent masses, via the dotted curve. We note that “small” random volumes, roughly at or below Milky Way masses, exhibit a sharp excess of  $\Delta t_{\text{reion}} \lesssim 10$  Myr. This indicates that most random  $\lesssim 10^{12} M_{\odot}$  regions are reionized essentially uniformly and likely have relatively little reionization structure. Going to higher mass bins, this sharp peak in the distribution slowly widens and essentially disappears in the  $\sim 10^{14} M_{\odot}$  bin, giving way to a broader distribution of more extended  $\Delta t_{\text{reion}}$ . The fact that there is still a fairly broad spread of  $\Delta t_{\text{reion}}$  for random cluster-mass volumes implies that reionization histories and reionization structure are quite variable from region to region, even on these large scales.

While the mean  $\Delta t_{\text{reion}}$  within a given halo mass bin does not appear to be a strong function of halo mass, if at all, we nevertheless find that smaller halos have a broader range of  $\Delta t_{\text{reion}}$ , implying a marked halo-to-halo diversity in reionization histories and scenarios. In particular, Milky Way mass halos exhibit  $\Delta t_{\text{reion}}$  of anywhere from  $\sim 1$  Myr to  $\sim 300$  Myr. In the next section, we specifically focus on the connection between  $\Delta t_{\text{reion}}$  and environment for  $10^{12 \pm 0.25} M_{\odot}$  halos.

### 3.2. Reionization and Large Scale Environment

Figure 4 shows localized slices through the reionization cube, centered on the regions which collapse into present-day Milky Way mass halos, selected to show those with the longest and shortest  $\Delta t_{\text{reion}}$ . MW halos with the shortest  $\Delta t_{\text{reion}}$  form in regions which ionize slightly earlier overall, whereas MW halos with the longest  $\Delta t_{\text{reion}}$  are surrounded by regions which do not ionize until quite late. Furthermore, Figure 5 shows the same 10 MW halos in the context of their *present-day* surroundings, with each nearby halo marked with its own  $\Delta t_{\text{reion}}$ . While these slices show only the most extreme cases, they suggest that halos with the shortest  $\Delta t_{\text{reion}}$

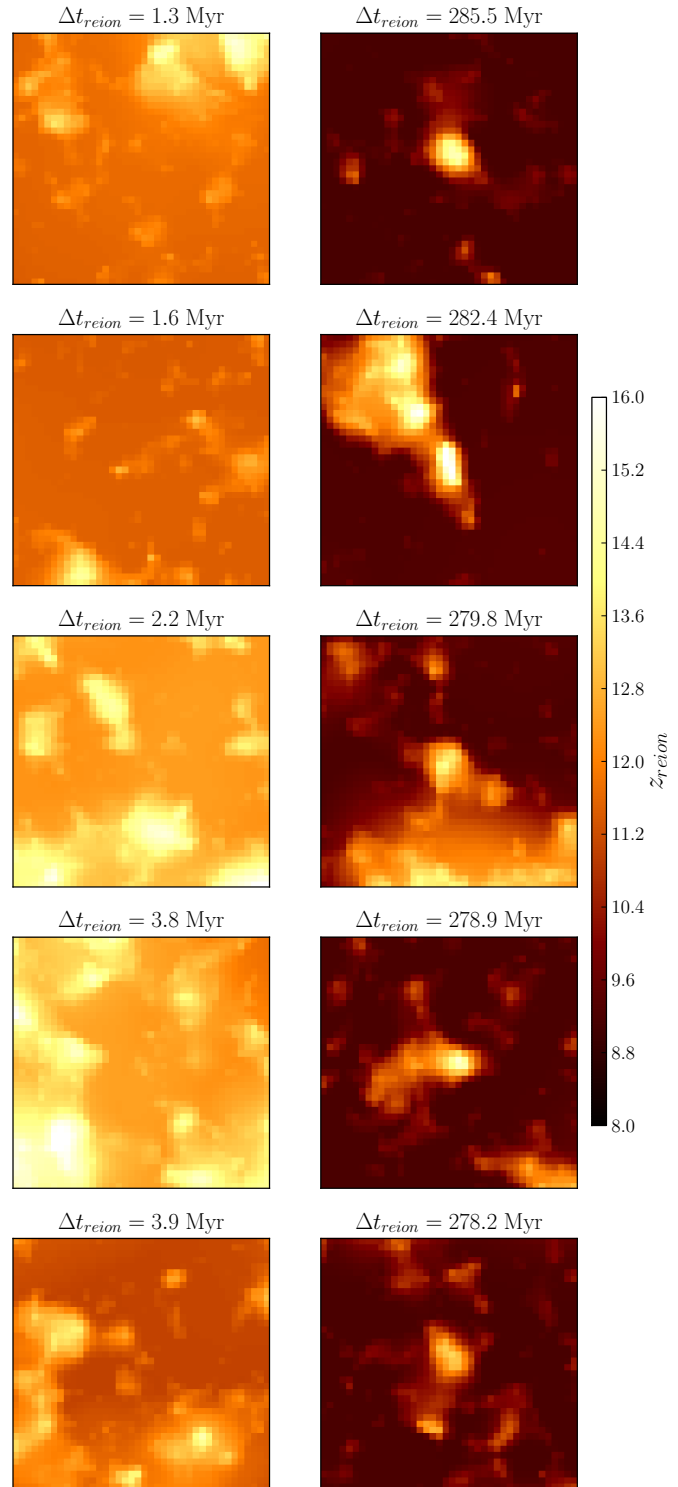


FIG. 4.— Slices through the 3D reionization map, centered on the *initial* center of mass of particles in eventual  $z = 0$  Milky Way mass halos ( $10^{12 \pm 0.25} M_{\odot}$ ). Plotted are mean-value projections, through a slice with comoving dimensions:  $12.3 \times 12.3 \times 3.3 \text{ Mpc } h^{-1}$ . Note that each cell coincides with the initial, unperturbed position of a particle. Reionization environments are shown for halos with the (left) shortest and (right) longest  $\Delta t_{\text{reion}}$ .

are found in more clustered environments, and are themselves

surrounded by halos with relatively short  $\Delta t_{\text{reion}}$ . By contrast, halos with the longest  $\Delta t_{\text{reion}}$  are apparently found in relative isolation, and the few halos which surround them also tend to have relatively long  $\Delta t_{\text{reion}}$ .

Figure 6 displays the distribution of  $\Delta t_{\text{reion}}$  for MW halos, binned by the abundance of nearby halos (specifically, nearby halos larger than the cutoff  $10^{11.75} M_{\odot}$ , within 20 Mpc, at  $z=0$ ). The median  $\Delta t_{\text{reion}}$  ranges from  $\sim 200$  Myr for halos in highly isolated environments to  $\sim 75$  Myr for halos in highly clustered environments.

That MW halos with short  $\Delta t_{\text{reion}}$  are preferentially found in clustered environments suggests a physical picture for those halos' reionization processes: namely, that MW halos with short  $\Delta t_{\text{reion}}$  contain more “externally” reionized matter, which was ionized by radiation from sources outside of the halo progenitors. Within the context of our reionization model, we define “internally” and “externally” reionized particles following a criterion proposed by Alvarez et al. (2009). We are able to assign each halo particle two characteristic radii:

1.  $R_{\text{bubble}}$ , the radius of the region at which it first crossed the ionization threshold, and
2.  $R_{\text{Lag}}$ , the  $z=0$  halo's Lagrangian radius, defined by  $M_{\text{halo}} = 4\pi\bar{\rho}R_{\text{Lag}}^3/3$ .

We consider the particle internally reionized if  $R_{\text{bubble}} < R_{\text{Lag}}$ , and externally reionized if  $R_{\text{bubble}} > R_{\text{Lag}}$ . We can thus obtain a halo's internally reionized mass fraction,  $f_{\text{internal}}$ .

Figure 7 shows the correlation between  $f_{\text{internal}}$  and  $\Delta t_{\text{reion}}$ , as well as between  $f_{\text{internal}}$  and the abundance of nearby ( $< 20$  Mpc) halos (rank correlation coefficients:  $\rho = 0.64$  and  $\rho = -0.38$ , respectively). Halos with short reionization histories preferentially contain more externally reionized mass, and more externally reionized halos tend to be found in clustered environments.

### 3.3. Milky Way Environmental Constraints: M31 and Virgo

Naturally, one wishes to determine where to place the true Milky Way halo in the aforementioned distributions. There exist numerous previous studies which have selected Milky Way candidates from simulations by matching, for example, the observed mass, velocity, and distance properties of the Local Group, the presence of the Virgo Cluster, and/or the local number density of observable galaxies (e.g., Governato et al. 1997; Forero-Romero et al. 2011; Schlegel et al. 1994; Few et al. 2012). A comprehensive investigation of the connection between the true Local Group environment and its reionization history is warranted but is left for future study. As an exploratory check, we select out candidates based on distance constraints to M31 and the Virgo Cluster. The following criteria were separately used:

1. MW mass halos  $750 \pm 50$  kpc away from exactly one other  $10^{12 \pm 0.25} M_{\odot}$  halo, corresponding to a MW-M31 distance constraint.
2. MW mass halos  $16.5 \pm 1.1$  Mpc away from exactly one  $\sim 10^{14.4 \pm 0.25} M_{\odot}$  halo, corresponding to a MW-Virgo Cluster constraint.

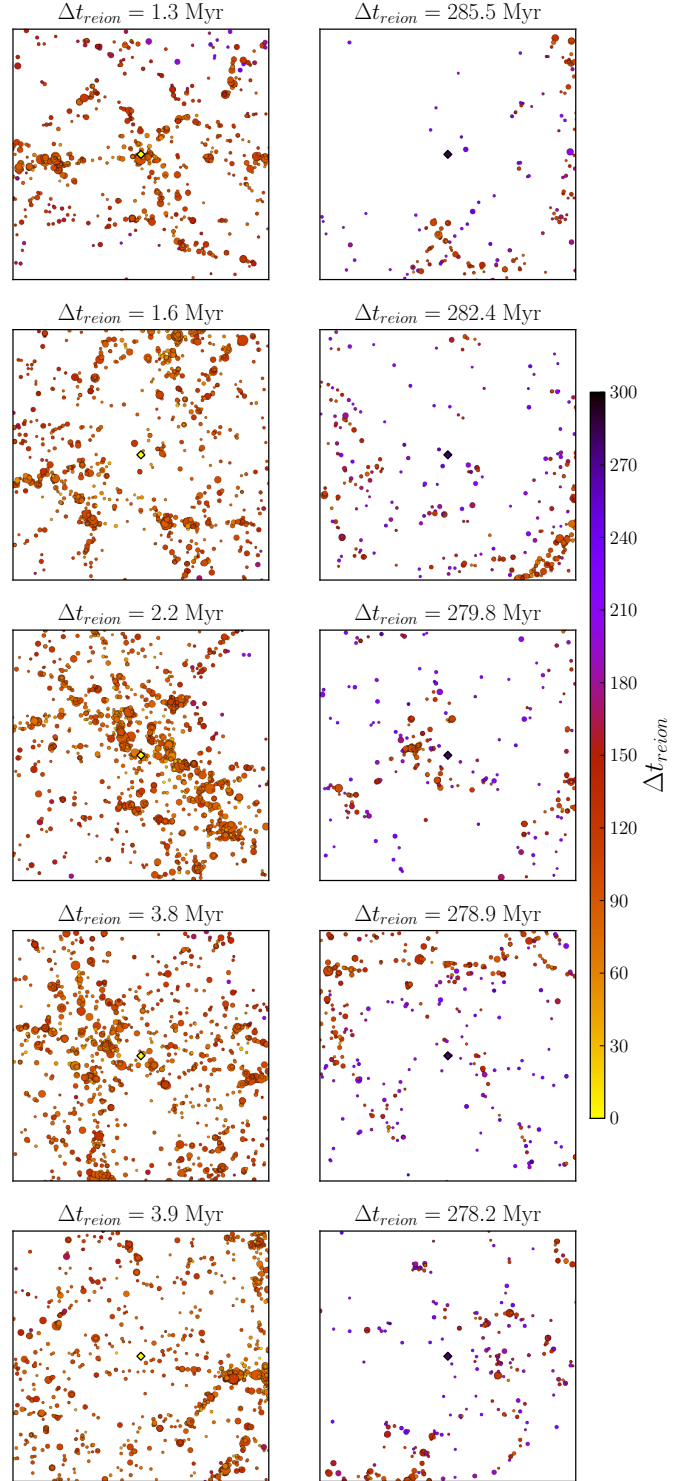


FIG. 5.— Present day surroundings of MW-mass halos, with the (left) 5 shortest and (right) 5 longest  $\Delta t_{\text{reion}}$ . Each plot represents a 2D projection of a rectangular volume,  $50 \times 50 \times 20 \text{ Mpc } h^{-1}$ , centered around the  $z=0$  halo of note (diamond). Surrounding halos (circles) are themselves colored by their  $\Delta t_{\text{reion}}$ . Only halos with mass  $> 10^{11.75} M_{\odot}$  are shown. Note: circle sizes scale monotonically with halo mass and do not directly represent physical halo size.

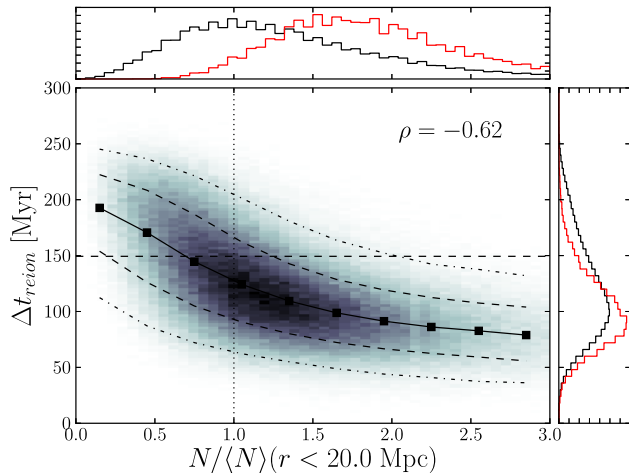


FIG. 6.— 2D histogram of  $\Delta t_{\text{reion}}$  vs. the overdensity of neighboring halos (within 20 Mpc), for present-day Milky Way mass halos. Note that only  $10^{12 \pm 0.25} M_{\odot}$  halos are histogrammed, but any halo larger than  $10^{11.75} M_{\odot}$  can be counted as one of their neighboring halos. Lines plot the median trend (solid), as well as the  $1\sigma$  (dashed) and  $2\sigma$  (dash-dotted) spread. The Spearman rank correlation coefficient  $\rho$  is also indicated. The horizontal dashed line represents  $\Delta t_{\text{reion}}$  for the entire box, while the vertical dotted line explicitly marks the mean number density of halos. Individual 1D distributions are also shown, both for all MW mass halos (black) and those located near a Virgo mass halo (red, see Section 3.3).

### 3. MW mass halos which satisfy both of the previous constraints.

The distance constraints, while deliberately lenient, are consistent with measured values from the literature (e.g., McConnachie et al. 2005; Mei et al. 2007). From our full sample of 383,237 Milky Way mass halos, the M31-only constraint selected out 1.7% of the sample, the Virgo-only constraint selected about 7.0%, and the combined M31-Virgo constraint selected out 0.12% (458 candidate halos). Including M31 in our criteria (Constraints 1 and 3) did not statistically change any of the distributions presented here. The Virgo-only constraint (Constraint 2) does have a noticeable effect, as indicated by the red 1-D distributions in Figures 6 and 7: from the full sample, it selects out MW halos with a typically higher local overdensity, shorter reionization history, and slightly lower internally reionized mass fraction.

The masses of our Virgo candidates are consistent with a range of measured values,  $(1.4 - 4.2) \times 10^{14} M_{\odot}$  (Ferrarese et al. 2012), though we note that there is significant uncertainty in these measurements. Increasing the mass of Virgo candidates selects even more preferentially for MW halos that have shorter reionization histories, are in more overdense environments, and have lower  $f_{\text{internal}}$ .

The presence of Virgo is of particular interest since its progenitors may have reionized some or much the present-day Local Group (e.g. Weinmann et al. 2007; Alvarez et al. 2009). Since we find that Milky Way halos near a Virgo-like cluster typically have slightly more externally reionized matter, it is plausible that Virgo was responsible for externally reionizing at least some material in the Milky Way.

### 3.4. Varying Reionization Model Parameters

Figure 8 displays the values of  $\Delta t_{\text{reion}}$  obtained for Milky Way mass halos, over all combinations of parameter values in

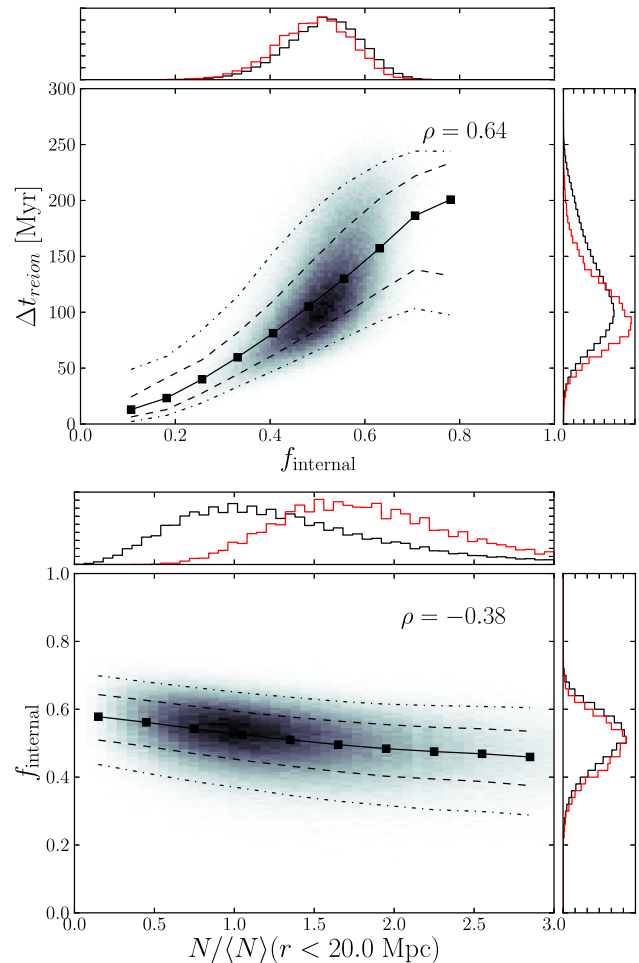


FIG. 7.— Correlations between  $f_{\text{internal}}$  and both variables from Figure 6 ( $\Delta t_{\text{reion}}$  and local halo number density). See that figure for more details. Individual 1D distributions are also shown, both for all MW mass halos (black) and those located near a Virgo mass halo (red, see Section 3.3). **Top:** 2D histogram of  $\Delta t_{\text{reion}}$  vs.  $f_{\text{internal}}$ , the fraction of “internally” reionized mass for present-day MW halos. **Bottom:** 2D histogram of  $f_{\text{internal}}$  vs. the number density of halos within 20 Mpc, for present-day MW halos.

our reionization model. Holding all other parameters fixed, decreasing  $\tau_{\text{es}}$  to 0.06 increases the median MW  $\Delta t_{\text{reion}}$  to  $\sim 240$  Myr, and increasing  $\tau_{\text{es}}$  to 0.12 decreases the median MW  $\Delta t_{\text{reion}}$  to  $\sim 60$  Myr. The strong decrease in reionization duration with increasing  $\tau_{\text{es}}$  is due mainly to the shorter Hubble time for earlier reionization. Increasing  $M_{\text{min}}$  independently to  $10^9 M_{\odot}$  also shortens  $\Delta t_{\text{reion}}$  in MW halos to  $\sim 70$  Myr. This is because higher mass halos are rarer, and therefore grow in abundance more quickly at a given redshift, leading to a shorter reionization duration.

Varying  $\lambda_{\text{abs}}$  over the values  $(8, 32, 256) \text{ Mpc } h^{-1}$  appears to have little to no systematic effect on the  $1\sigma$  spread of  $\Delta t_{\text{reion}}$  values for MW halos. This is expected, mainly for two reasons. First, as shown by Alvarez & Abel (2012), the absorption system mean free path affects the final percolation phase of reionization, when the global neutral fraction is less than  $\sim 0.1$ . Given that our definition of the duration of reionization is the range over which  $0.16 < x < 0.84$ , on average the duration of reionization within individual halos should not change

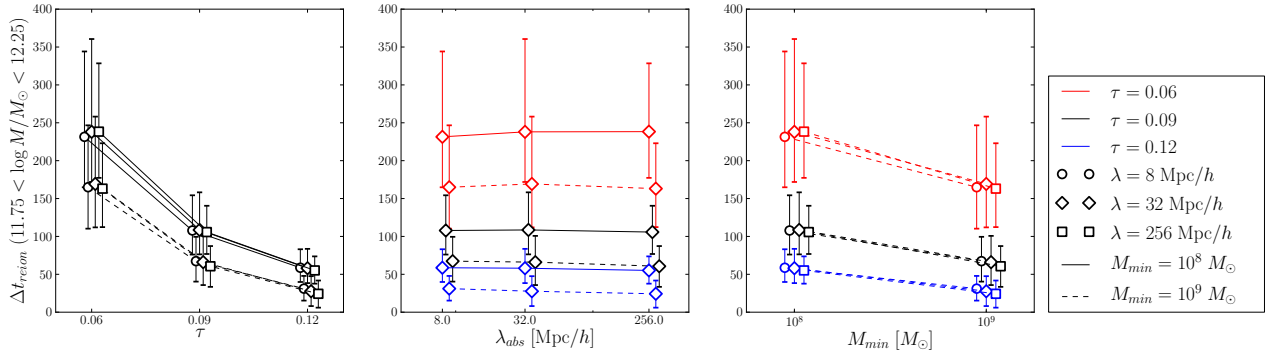


FIG. 8.— Values of  $\Delta t_{\text{reion}}$  for Milky Way mass halos, over different reionization parameter values. Median values (points) and  $1\sigma$  spread (error bars) are shown for each combination of  $\tau_{\text{es}}$ ,  $\lambda_{\text{abs}}$ , and  $M_{\text{min}}$ . In each panel, a different parameter is independently varied on the horizontal axis, but each panel contains the same 18 points and error bars. Point have been plotted with a slight horizontal offset for readability. **Left:** Variation of  $\Delta t_{\text{reion}}$  with  $\tau_{\text{es}}$ , the optical depth to reionization. In general, higher values of  $\tau_{\text{es}}$  correspond to earlier reionization scenarios. **Middle:** Variation of  $\Delta t_{\text{reion}}$  with  $\lambda_{\text{abs}}$ , the mean free path of Lyman absorption systems. **Right:** Variation of  $\Delta t_{\text{reion}}$  with  $M_{\text{min}}$ , the minimum halo mass of ionizing sources.

much. Second, while smaller  $\lambda_{\text{abs}}$  introduces more inhomogeneous reionization structure on the scale of  $\sim \lambda_{\text{abs}}$ , even scales of  $\lambda_{\text{abs}} \sim 8 \text{ Mpc } h^{-1}$  are still well outside the  $\sim 1 \text{ Mpc } h^{-1}$  Lagrangian radii of  $10^{12} M_{\odot}$  halos. Those MW halos that are reionized internally therefore are not sensitive to changes in the mean free path  $\lambda_{\text{abs}}$ . Further work will be required to assess the effect of varying  $\lambda_{\text{abs}}$  on externally reionized halos.

We find that the inverse correlation of  $\Delta t_{\text{reion}}$  with abundance of nearby halos is present in all models. However, in scenarios that combine high values of  $\tau_{\text{es}}$  and  $M_{\text{min}}$  ( $\tau_{\text{es}} = 0.09, 0.12$  and  $M_{\text{min}} = 10^9 M_{\odot}$ ), we find many MW mass halos with  $\Delta t_{\text{reion}} \approx 0$ . This indicates a significant population of such halos with highly homogeneous reionization histories, for these particular reionization scenarios. Such models, however, are at the extreme end of our parameter space and are disfavoured – if  $\tau_{\text{es}} > 0.09$ , it is more likely that the reionization history is more complex than the models presented here, perhaps due to photoionization feedback (Iliev et al. 2007; Alvarez et al. 2012, e.g.), substantial early ionization by massive stars in minihalos (e.g., Abel et al. 2007; Ahn et al. 2012), or even pre-reionization by x-rays (e.g., Ricotti & Ostriker 2004; Ricotti et al. 2005; McQuinn 2012).

#### 4. DISCUSSION

We have simulated the reionization of a 600 Mpc box and characterized reionization histories of  $z = 0$  halos, focusing on Milky Way mass halos and the dependence of  $\Delta t_{\text{reion}}$  on environment. Our main results are as follows:

1. We quantify the typical spread in reionization epochs within  $z = 0$  halos. In our fiducial reionization model, we find that in our smallest halos,  $\sim 10^{11.5} M_{\odot}$ , the median scatter in reionization times is  $\Delta t_{\text{reion}} \sim 100$  Myr. In Milky Way mass halos,  $\sim 10^{12} M_{\odot}$ , this increases slightly to  $\Delta t_{\text{reion}} \sim 115$  Myr. For the largest cluster mass halos,  $\sim 10^{15} M_{\odot}$ , this decreases slightly to  $\Delta t_{\text{reion}} \sim 95$  Myr.
2. The typical scatter of reionization epochs *within halos* is notably larger than the scatter *across halos*, provided the “reionization epoch” of a single halo is defined by its median reionization time. This is true for all halo

masses considered in this study. To be explicit, the scatter *across* halos is  $\sim 90$  Myr for  $\sim 10^{11.5} M_{\odot}$  halos, decreasing to  $\sim 10$  Myr for  $\sim 10^{15} M_{\odot}$  halos.

3. For MW mass halos, the halo-to-halo diversity in  $\Delta t_{\text{reion}}$  is significant (ranging at the extremes from  $\sim 1$  Myr to  $\sim 286$  Myr). The values of  $\Delta t_{\text{reion}}$  for individual halos correlate with both their reionization environments and present-day environments. MW mass halos with short (long)  $\Delta t_{\text{reion}}$  were formed from regions which reionized relatively homogeneously (inhomogeneously) and slightly earlier (later). They also tend to be found in clustered (isolated) present-day environments, i.e. they are surrounded by relatively more (fewer) halos within a radius of 20 Mpc. A larger fraction of their mass is likely to have been externally (internally) reionized.
4. Varying the global parameters of the reionization model will affect the  $\Delta t_{\text{reion}}$  values in MW mass halos. Increasing  $\tau_{\text{es}}$  decreases the typical  $\Delta t_{\text{reion}}$ . Increasing  $M_{\text{min}}$  also decreases the typical  $\Delta t_{\text{reion}}$ . Varying  $\lambda_{\text{abs}}$  has little to no systematic effect on the typical  $\Delta t_{\text{reion}}$  values of MW mass halos.

Our results suggest that the reionization histories of present-day halos are inadequately characterized by a single  $z_{\text{reion}}$ , and this has potential implications for modeling the satellite galaxies of the Milky Way. For simplicity, a single  $z_{\text{reion}}$  has often been assumed in galaxy formation models (e.g. Koposov et al. 2009; Busha et al. 2010). Under such an assumption, Busha et al. (2010) found that the timing of the reionization epoch may strongly affect the present-day Milky Way satellite population, with the number varying by up to two orders of magnitude over the reionization epochs  $z_{\text{reion}} \approx 6 - 12$ . However, using a single  $z_{\text{reion}}$  per halo implicitly assumes that scatter of reionization times within halos is smaller than the scatter across halos. Our results suggest otherwise: the spread of reionization times within halos is *not* negligible compared to the spread of (median) reionization times across halos. This result would thus reduce the predicted halo-to-halo variation in satellite populations across Milky Way mass halos.



In other words,  $\Delta t_{\text{reion}}$  is essential to fully characterize the impact of reionization on the  $z = 0$  halo, with the minority exception of halos that were reionized rapidly, likely by external sources. We did find that in scenarios combining high  $\tau_{\text{es}}$  (0.09, 0.12) and  $M_{\text{min}}$  ( $10^9 M_{\odot}$ ), there were many MW mass halos with short  $\Delta t_{\text{reion}}$ , as compared to the halo-to-halo scatter. In these scenarios—corresponding to relatively early reionization by rare but highly efficient ionizing sources—many MW mass halos would be better characterized by a single reionization epoch,  $z_{\text{reion}}$ , than by a spread,  $\Delta t_{\text{reion}}$ .

Notably, we find a correlation between the reionization history of Milky Way halos and their environment, as well as their fraction of internally reionized mass (Figures 6 and 7). This contrasts somewhat with the results of Weinmann et al. (2007), which found no statistical correlation between reionization histories of field halos—either in terms of reionization epoch or the number of externally reionized halos—and their environment. However, it is worth pointing out that our definitions differ from theirs. Rather than a binary definition of an internally vs. externally reionized halo, we defined an internally reionized mass fraction for each halo, which does correlate with reionization history and environment. Our criteria for internally vs. externally reionized mass is also fundamentally different, owing partly to a difference in reionization model. Additionally, we have characterized halo reionization histories differently, noting that most are more accurately characterized by  $\Delta t_{\text{reion}}$  rather than a single epoch  $z_{\text{reion}}$ .

The values of  $\Delta t_{\text{reion}}$  found here are likely to be lower limits. This is because our model does not self-consistently include or treat photoheating feedback in galaxy formation, which could act as a self-regulation mechanism by suppressing ionizing radiation released by halos in already-reionized regions. Additionally, in this model, once a cell crosses the reionization threshold, it remains ionized: this would not account for so-called relic HII regions, which might form around short-lived early sources (e.g., Wise & Abel 2008), or other multiply reionized regions. We also note that  $\lambda_{\text{abs}}$  in this model is, for simplicity, both spatially uniform and constant in time, while in reality it is likely to be neither. We leave fully self-consistent treatments of absorption systems to future studies, although we reiterate that varying  $\lambda_{\text{abs}}$  did not

significantly affect the specific findings we presented here.

Observationally, the reionization history of the Milky Way might be imprinted in its satellite population. For example, if star formation histories in at least some ultra-faint dwarfs were suddenly truncated during reionization (Brown et al. 2012), and one obtained a statistical sample of such satellites, then the spread in their truncation epochs should correspond to  $\Delta t_{\text{reion}}$  of the Milky Way. However, such truncation epochs would need to be determined at a precision of  $\lesssim 50$  Myr, well below the current  $\sim$  Gyr uncertainties quoted in Brown et al. (2012).

The local reionization history could also affect the number of faint satellite galaxies. As previously noted, earlier reionization could suppress star formation and decrease the number of faint satellites, but the effect of varying  $\Delta t_{\text{reion}}$  on any individual halo is unclear without further knowledge of environment and assembly history. When comparing instantaneous and inhomogeneous reionization scenarios, Lunnan et al. (2012) found no systematic offset in  $N_{\text{sat}}(M_V \gtrsim -10)$ , while acknowledging their small sample size of 6 Milky Way halos. Here, we have characterized the reionization histories of a large sample of Milky Way mass halos, at the expense of resolving their internal substructures. Further study, retaining a statistically significant sample of halos while resolving their subhalos, will be necessary to fully understand the impact of patchy reionization on the satellite population of Milky Way halos.

TYL is supported by a National Science Foundation Graduate Research Fellowship. This work received support from the National Science Foundation under grant NSF-AST-0908883. We thank Michael Busha for several useful discussions, and, along with the rest of the LasDamas collaboration for providing access to the Las Damas simulations, which were run on the Orange cluster at SLAC and on the NSF TeraGrid machine Ranger (PI: Andreas Berlind). The reionization simulations were performed in part on the GPC supercomputer at the SciNet HPC Consortium. SciNet is funded by: the Canada Foundation for Innovation under the auspices of Compute Canada, the Government of Ontario, Ontario Research Fund—Research Excellence, and the University of Toronto. We also thank Marla Geha for helpful discussions and comments.

#### REFERENCES

- Abel, T., Wise, J. H., & Bryan, G. L. 2007, *ApJ*, 659, L87  
Ahn, K., Iliiev, I. T., Shapiro, P. R., et al. 2012, *ApJ*, 756, L16  
Alvarez, M. A., & Abel, T. 2012, *ApJ*, 747, 126  
Alvarez, M. A., Busha, M., Abel, T., & Wechsler, R. H. 2009, *ApJ*, 703, L167  
Alvarez, M. A., Finlator, K., & Trenti, M. 2012, *ApJ*, 759, L38  
Barkana, R., & Loeb, A. 1999, *ApJ*, 523, 54  
—. 2004, *ApJ*, 609, 474  
Becker, R. H., Fan, X., White, R. L., et al. 2001, *AJ*, 122, 2850  
Behroozi, P. S., Wechsler, R. H., & Wu, H.-Y. 2013, *ApJ*, 762, 109  
Belokurov, V., Zucker, D. B., Evans, N. W., et al. 2007, *ApJ*, 654, 897  
Bennett, C. L., Larson, D., Weiland, J. L., et al. 2012, *ArXiv e-prints*, arXiv:1212.5225  
Bond, J. R., Cole, S., Efstathiou, G., & Kaiser, N. 1991, *ApJ*, 379, 440  
Bouwens, R. J., Illingworth, G. D., Oesch, P. A., et al. 2012, *ApJ*, 752, L5  
Brown, T. M., Tumlinson, J., Geha, M., et al. 2012, *ApJ*, 753, L21  
Bullock, J. S., Kravtsov, A. V., & Weinberg, D. H. 2000, *ApJ*, 539, 517  
Busha, M. T., Alvarez, M. A., Wechsler, R. H., Abel, T., & Strigari, L. E. 2010, *ApJ*, 710, 408  
Dijkstra, M., Haiman, Z., Rees, M. J., & Weinberg, D. H. 2004, *ApJ*, 601, 666  
Efstathiou, G. 1992, *MNRAS*, 256, 43P  
Fan, X., Carilli, C. L., & Keating, B. 2006, *ARA&A*, 44, 415  
Ferrarese, L., Côté, P., Cuillandre, J.-C., et al. 2012, *ApJS*, 200, 4  
Few, C. G., Gibson, B. K., Courty, S., et al. 2012, *A&A*, 547, A63  
Forero-Romero, J. E., Hoffman, Y., Yepes, G., et al. 2011, *MNRAS*, 417, 1434  
Furlanetto, S. R., & Oh, S. P. 2005, *MNRAS*, 363, 1031  
Furlanetto, S. R., Zaldarriaga, M., & Hernquist, L. 2004, *ApJ*, 613, 1  
Gnedin, N. Y. 2000a, *ApJ*, 535, 530  
—. 2000b, *ApJ*, 542, 535  
Governato, F., Moore, B., Cen, R., et al. 1997, *New Astron.*, 2, 91  
Hinshaw, G., Larson, D., Komatsu, E., et al. 2012, *ArXiv e-prints*, arXiv:1212.5226  
Iliiev, I. T., Mellema, G., Pen, U.-L., et al. 2006, *MNRAS*, 369, 1625  
Iliiev, I. T., Mellema, G., Shapiro, P. R., & Pen, U.-L. 2007, *MNRAS*, 376, 534  
Iliiev, I. T., Moore, B., Gottlöber, S., et al. 2011, *MNRAS*, 413, 2093

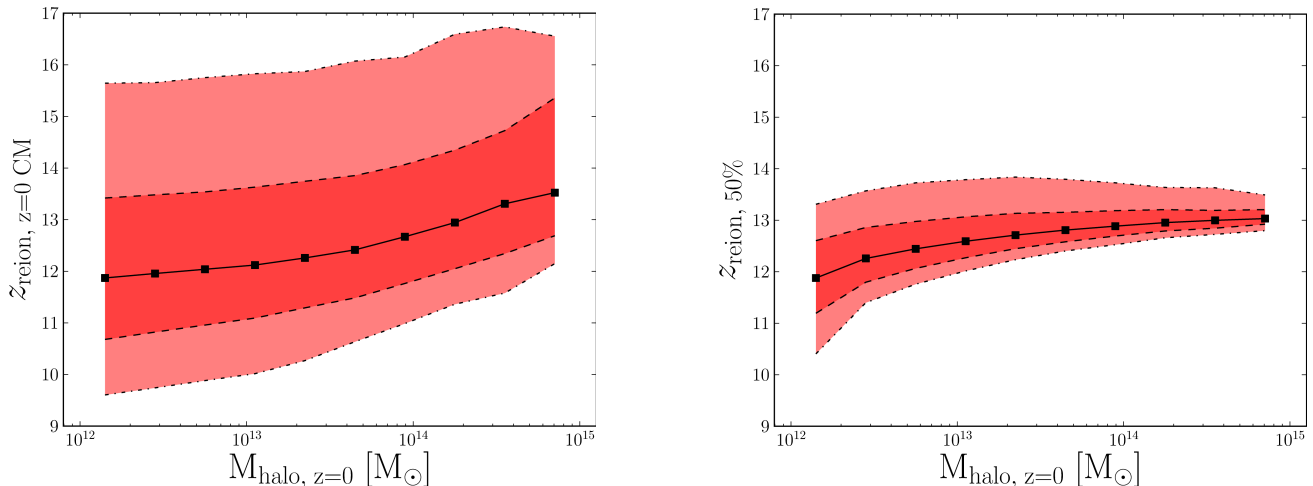


FIG. 9.— **Left:** Halo reionization redshifts, as a function of halo mass, using  $z_{\text{reion}}$  of the  $z = 0$  halo center of mass. **Right:** Median halo reionization redshifts, as a function of  $z = 0$  halo mass. Plotted in both are the median trend (solid black), as well as the 68% (dashed) and 95% (dot-dashed) distributions.

Klypin, A., Kravtsov, A. V., Valenzuela, O., & Prada, F. 1999, *ApJ*, 522, 82  
 Komatsu, E., Smith, K. M., Dunkley, J., et al. 2011, *ApJS*, 192, 18  
 Kogosov, S. E., Yoo, J., Rix, H.-W., et al. 2009, *ApJ*, 696, 2179  
 Kravtsov, A. V., Gnedin, O. Y., & Klypin, A. A. 2004, *ApJ*, 609, 482  
 Kuhlen, M., & Faucher-Giguère, C.-A. 2012, *MNRAS*, 423, 862  
 Lacey, C., & Cole, S. 1993, *MNRAS*, 262, 627  
 Lunnan, R., Vogelsberger, M., Frebel, A., et al. 2012, *ApJ*, 746, 109  
 McConnachie, A. W., Irwin, M. J., Ferguson, A. M. N., et al. 2005, *MNRAS*, 356, 979  
 McQuinn, M. 2012, *MNRAS*, 426, 1349  
 Mei, S., Blakeslee, J. P., Côté, P., et al. 2007, *ApJ*, 655, 144  
 Mesinger, A., & Furlanetto, S. 2007, *ApJ*, 669, 663  
 Mesinger, A., Furlanetto, S., & Cen, R. 2011, *MNRAS*, 411, 955  
 Miralda-Escudé, J., Haehnelt, M., & Rees, M. J. 2000, *ApJ*, 530, 1  
 Moore, B., Ghigna, S., Governato, F., et al. 1999, *ApJ*, 524, L19  
 Ocvirk, P., & Aubert, D. 2011, *MNRAS*, 417, L93  
 Okamoto, T., Gao, L., & Theuns, T. 2008, *MNRAS*, 390, 920  
 Planck Collaboration, Ade, P. A. R., Aghanim, N., et al. 2013, *ArXiv e-prints*, arXiv:1303.5062  
 Ricotti, M., & Ostriker, J. P. 2004, *MNRAS*, 352, 547  
 Ricotti, M., Ostriker, J. P., & Gnedin, N. Y. 2005, *MNRAS*, 357, 207

Santos, M. G., Ferramacho, L., Silva, M. B., Amblard, A., & Cooray, A. 2010, *MNRAS*, 406, 2421  
 Schlegel, D., Davis, M., Summers, F., & Holtzman, J. A. 1994, *ApJ*, 427, 527  
 Shapiro, P. R., Giroux, M. L., & Babul, A. 1994, *ApJ*, 427, 25  
 Shin, M.-S., Trac, H., & Cen, R. 2008, *ApJ*, 681, 756  
 Sokasian, A., Abel, T., & Hernquist, L. E. 2001, *New Astron.*, 6, 359  
 Springel, V. 2005, *MNRAS*, 364, 1105  
 Thoul, A. A., & Weinberg, D. H. 1996, *ApJ*, 465, 608  
 Trac, H., & Cen, R. 2007, *ApJ*, 671, 1  
 Weinmann, S. M., Macciò, A. V., Iliiev, I. T., Mellema, G., & Moore, B. 2007, *MNRAS*, 381, 367  
 Willman, B., Blanton, M. R., West, A. A., et al. 2005, *AJ*, 129, 2692  
 Wise, J. H., & Abel, T. 2008, *ApJ*, 684, 1  
 Wise, J. H., & Cen, R. 2009, *ApJ*, 693, 984  
 Zahn, O., Lidz, A., McQuinn, M., et al. 2007, *ApJ*, 654, 12  
 Zahn, O., Mesinger, A., McQuinn, M., et al. 2011, *MNRAS*, 414, 727  
 Zahn, O., Zaldarriaga, M., Hernquist, L., & McQuinn, M. 2005, *ApJ*, 630, 657  
 Zucker, D. B., Belokurov, V., Evans, N. W., et al. 2006, *ApJ*, 650, L41

## APPENDIX

### HALO REIONIZATION REDSHIFTS

Here we further discuss the assertion that halo reionization histories, for masses considered in this study, are inadequately characterized by a single reionization redshift. In particular, we expand on Alvarez et al. (2009), in which each halo was assigned a reionization redshift corresponding to the comoving cell around its  $z = 0$  center of mass (CM). This was justified by asserting that most halos would not achieve sufficiently high peculiar velocities to displace the halo CM out of the original ionizing bubble region. The left plot of Figure 9 shows the distribution of halo  $z_{\text{reion}}$  in this study, by this definition, as a function of mass.

However, if the particles of all  $z = 0$  halos are tracked over the course of the entire simulation, the last panel of Figure 10 shows the distribution of their total CM displacements, after correcting for boundary periodicity, as a function of mass. From the plot, it is apparent that the distribution is relatively consistent over all halo masses in this study. Evidently, the typical comoving CM displacement is  $\sim 8 \text{ Mpc } h^{-1}$ , or  $\sim 25$  cells in our reionization cube, but significantly larger displacements are not uncommon. Thus, while present-day massive halos are preferentially found in overdense regions, which correlate with earlier reionization redshifts, the  $z_{\text{reion}}$  values thus obtained are not necessarily indicative of the reionization redshift of matter *presently* in the halo, especially for smaller halos. Even if they are, such values of halo  $z_{\text{reion}}$  are subject to scatter across halos that is comparable to the scatter in  $z_{\text{reion}}$  within halos, and so it is generally unclear whether a single such  $z_{\text{reion}}$  for an entire halo characterizes the beginning, middle, or end of its reionization history.

A more consistent marker might be redshift at which the halo mass is 50% reionized,  $z_{\text{reion}, 50\%}$ , but we find that this correlates more weakly with halo mass in the mass range  $10^{12} M_{\odot} < M_{\text{halo}} < 10^{15} M_{\odot}$ , as shown in the second panel of Figure 9. We interpret this trend to indicate that more massive present day halos are still generally correlated with regions of earlier reionization. However, we interpret the weakness of the trend and the narrowness of the distribution at high masses (approaching  $\sim 10^{15} M_{\odot}$ ) by invoking hierarchical structure formation. Present-day halos were generally built up from small halos via mergers, many of

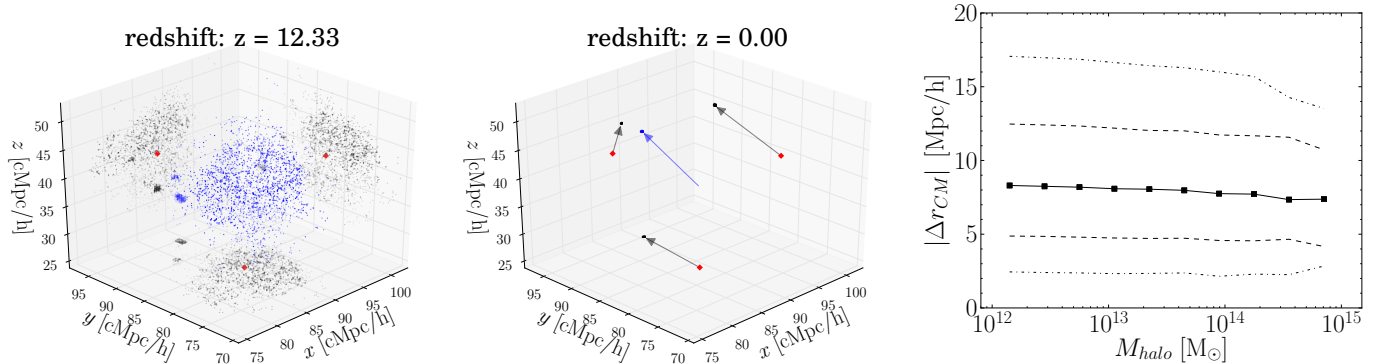


FIG. 10.— **Left:** Particles of a randomly selected present-day halo, but in their positions at redshift  $z = 12.33$ . Shown here are particle positions in 3D (*blue points*), projections on the  $xy$ -,  $yz$ -, and  $xz$ - planes (*gray points*), and the projected initial center of mass (*red diamonds*). **Middle:** Same halo particles at redshift  $z = 0$ , with the projected initial center of mass (*red diamonds*) retained for reference. Arrows indicate the 3D (*blue*) and projected (*gray*) total displacement of the center of mass. **Right:** Total center-of-mass displacement of  $z = 0$  halos, as a function of mass. The solid line follows the median in each mass bin, while the dashed and dash-dotted lines follow the 68% and 95% distributions, respectively.

which occurred after reionization. While the reionization histories of distinct halos at the end of reionization may vary greatly,  $z = 0$  halos aggregate those once-separate reionization histories. More massive halos have aggregated more disparate reionization histories from a much larger Lagrangian region, and so the halo-to-halo variation in their  $z_{reion, 50\%}$  values will be suppressed.